Chemical, physical and biological triggers of evolutionary conserved Bcl-xL-mediated apoptosis

Aleksandr Ianevski [1], Evgeny Kulesskiy [2], Klara Krpina [1], Guofeng Lou [3], Yahyah Aman [3], Andrii Bugai [4], Koit Aasumets [5], Yevhen Akimov [2], Daria Bulanova [2], Kiira Gildemann [5], Albert F. Arutyunyan [6], Olga Yu. Susova [7], Alexei L. Zhuze [6], Ping Ji [1], Wei Wang [1], Toril Holien [1,8], Marit Bugge [1], Eva Zusinaite [5], Valentyn Oksenych [1], Hilde Lysvand [1], Joachim M. Gerhold [5], Magnar Bjørås [1], Pål Johansen [9], Anders Waage [1,8], Caroline Heckman [2], Evandro F. Fang [3], Denis E. Kainov [1,2,5] *

[1] Department of Clinical and Molecular Medicine, Norwegian University of Science and Technology, Trondheim 7028, Norway.

[2] Institute for Molecular Medicine Finland, FIMM, University of Helsinki 00014, Finland

[3] Department of Clinical Molecular Biology, University of Oslo and Akershus University Hospital, Lørenskog 1478, Norway

[4] Department of Biochemistry and Developmental Biology, University of Helsinki, Helsinki 00014, Finland

[5] Institute of Technology, University of Tartu, Tartu 50090, Estonia

[6] Engelhardt Institute of Molecular Biology Russian Academy of Sciences, Moscow 119991, Russia

[7] Institute of Carcinogenesis, FSBI "N.N. Blokhin National Medical Research Center of Oncology", The Ministry of Health of the Russian Federation, Moscow, Russia

[8] Department of Hematology, St. Olav's University Hospital, 7030 Trondheim, Norway

[9] Department of Dermatology, University of Zurich, Zurich, Switzerland

* To whom correspondence should be addressed. Tel: +358405490220; Fax: +358405490220; Email: denis.kainov@ntnu.no

ABSTRACT

The evidence that pan-Bcl-2 or Bcl-xL-specific inhibitors prematurely kill virus-infected or RNA/DNA-transfected cells provides rationale for investigating these apoptotic inducers further. Here, we show that Bcl-xL-specific agent A-1155463 prematurely kills cells of different origins and the small roundworms (*C. elegans*), when combined with DNA-damaging agent 4-nitroquinoline-1-oxide (4NQO). The synergistic effect of 4NQO-A-1155463 combination was p53-dependent, was associated with the release of Bad and Bax from Bcl-xL, which triggered mitochondrial outer membrane permeabilization (MOMP). Combinations of Bcl-xL-specific inhibitors with certain anticancer compounds or physical insults also killed cells. Collectively, our results suggest that biological, chemical and physical factors trigger evolutionary conserved Bcl-xL-mediated apoptotic pathway.

INTRODUCTION

Apoptosis is a tightly regulated process that kills cells with damaged or pathogenic DNA, RNA, and proteins (Elmore, 2007; Shim et al., 2017). When apoptosis is inhibited, cells that should be eliminated may persist and become malignant (Wong, 2011).

B cell lymphoma 2 (Bcl-2) family of proteins are key players in apoptosis (Kale et al., 2018). For example, Bcl-xL, Bcl-2 and Mcl-1 are anti-apoptotic, whereas Bax, Bak and Bad are pro-apoptotic members of the family (Denisova et al., 2012; Fernandez et al., 2018; Kuivanen et al., 2017). Interaction between pro- and anti-apoptotic proteins determine the fate of a cell. In particular, alteration of the interactions could lead to release of Bax and Bak which could form a pore in the mitochondrial outer membrane that allowed cytochrome C to escape into the cytoplasm and activate the caspase cascade (Shamas-Din et al., 2013).

Several chemical inhibitors were developed to bind anti-apoptotic of Bcl-2 proteins and induce cancer cells death including recently developed Bcl-PROTACs (Adams et al., 2018)(Khan, Zhang et al. 2019, Wang, He et al. 2019, He, Zhang et al. 2020). These small molecules belong to several structurally distinct classes (Fig. 1a). First class of Bcl-2 inhibitors (Bcl2i) includes ABT-737 and its derivatives, i.e. ABT-263 (navitoclax) and ABT-199 (venetoclax); second class includes WEHI-539 and its derivatives, A-1331852 and A-1155463. There are other classes of Bcl-2 inhibitors containing structurally similar molecules, such as S63845 and S64315, S55746 and A1210477.

The inhibitors have different affinities to Bcl-2 protein family members (Fig. 1b). For example, ABT-199 has a high affinity to Bcl-2; WEHI-539, A-1331852 and A-1155463 are specific for Bcl-xL; S63845, S64315, S55746 and A1210477 have high affinity to Mcl-1; whereas ABT-263 binds Bcl-2, Bcl-xL and Bcl-w with similar affinity. Importantly, ABT-199 was approved, whereas ABT-263, S63845 and several other Bcl-2 inhibitors are currently in clinical trials against blood cancers and solid tumours (Casara et al., 2018; King et al., 2017; Korycka-Wolowiec et al., 2019; Timucin et al., 2019) (NCT02920697). These drugs provide opportunities for treatment of hematologic and other types of cancers, but also create new challenges associated with emerging drug resistance of cancer cells and toxicity for non-cancer cells (e.g. thrombocytopaenia).

To obtain additive or synergistic effects, enhance efficacy of treatment and combat genetically heterogeneous cancers, Bcl-2 inhibitors were combined with other anticancer drugs (Fig. 1c; bcl2icombi.info) (Chen et al., 2011; Haikala et al., 2019; Jeong et al., 2019; Shen et al., 2018). The drug combinations were also used to lower the dose of Bcl-2 inhibitors to overcome resistance and toxicity issues for non-malignant cells (Adams et al., 2018). Dozens of the drug combinations have been reported to be active *in vitro* (cell culture, patient-derived cells or organoids) and *in vivo* (patient-derived xenograft mouse models). In addition, 109 combinations (excluding combinations with biological agents) were in clinical trials. However, only ABT-199 in combination with azacytidine, decitabine or cytarabine was approved for the treatment of acute myeloid leukaemia (AML).

We noticed that many Bcl-2 inhibitors have been combined with compounds, which damaged cellular macromolecules by targeting DNA replication, RNA transcription and decay, as well as protein signalling and degradation pathways. Here, we shed new light on the mechanisms of actions of such combinations. First, we showed that combination of DNA-damaging agent 4-nitroquinoline-1-oxide (4NQO) together with Bcl-xL-specific inhibitor A-1155463, but not drugs alone, killed human malignant and non-malignant cells, as well as *C. elegans*. The synergistic effect of the drug combination was p53-dependent. Moreover, it was associated with the release of Bad and Bax from Bcl-xL and

activation of MOMP. Second, we demonstrated that several anticancer drugs (i.e. amsacrine, SN38, cisplatin, mitoxantrone, dactinomycin, dinaciclib, UCN-01, bortezomib, and S63845) triggered Bcl-xl-mediated apoptosis in non-malignant cells. Third, we showed that combinations of Bcl-xL specific inhibitors with UV radiation also killed cells. Finally, we discussed the application of these results to cancer treatment.

METHODS

Bcl2iCombi.info database

We reviewed developmental status of Bcl-2 inhibitors and their combinations with other anticancer therapeutics. We summarized the information in freely accessible database (bcl2icombi.info). The drug annotations were obtained from PubChem, DrugBank, DrugCentral, PubMed and clinicaltrials.gov databases (Kim et al., 2019; Ursu et al., 2019; Wishart et al., 2018). The database summarizes activities and developmental stages of the drug combinations and allows their interactive exploration. A feedback form is available on the website. The database will be updated upon request or as soon as a new drug combination is reported.

Compounds

ABT-199 (CAS: 1257044-40-8), A-1331852 (CAS: 1430844-80-6), A-1155463 (CAS: 1235034-55-5), and S63845 (CAS: 1799633-27-4) were purchased from Selleck Chemicals (Houston, TX, USA). 4NQO (CAS: 56-57-5) was from Merck Life Science (Espoo, Finland). Dimeric bisbenzimidazoles DBA(3), DBA(5), DBA(7), monomeric MB2Py(Ac), dimeric DB2Py(4) and DB2Py(5) benzimidazole-pyrroles were synthesized as described previously (Ivanov et al., 2013; Koval et al., 2018). A library of 527 approved and emerging investigational oncology drugs were from the collection of the Institute of Molecular Medicine Finland, FIMM (www.fimm.fi/en/services/technology-centre/htb/equipment-and-libraries/chemical-libraries). A library of 48 drugs commonly dispensed in Norway was assembled based on Norwegian Prescription Database (www.norpd.no). Table S1 lists these compounds, their suppliers and catalogue numbers. A library of 50 safe-in-man broad-spectrum antivirals was published previously (Ianevski et al., 2018). To obtain 10 mM stock solutions, compounds were dissolved in dimethyl sulfoxide (DMSO, Sigma-Aldrich, Steinheim, Germany) or milli-Q water. The solutions were stored at −80 °C until use.

Cells

Human telomerase reverse transcriptase-immortalized retinal pigment epithelial (RPE, ATCC) and epithelial colorectal adenocarcinoma (Caco-2, ATCC) cells were grown in DMEM-F12 medium supplemented with 100 U/ml penicillin/streptomycin (Pen/Strep), 2 mM L-glutamine, 10% FBS, and 0.25% sodium bicarbonate (Sigma-Aldrich, St. Louis, USA). Human large-cell lung carcinoma NCI-H460 cells were grown in RPMI medium supplied with 10% FBS and Pen-Strep. Human adenocarcinoma alveolar basal epithelial cells (A549, ATCC) were grown in DMEM medium supplied

with 10% FBS and Pen-Strep. Human colon cancer cell lines HCT116 *TP53*$^{+/+}$ and HCT116 *TP53*$^{-/-}$ were grown in McCoy's 5A Medium (Sigma, M9309) supplemented with 10% FBS and Pen/Strep. The cell lines were maintained at 37°C with 5% CO2. Human colon cancer cell lines HT29 (ATCC, catalog no. HTB-38), SW620 (ATCC, catalog no. CCL-227) and SW480 (ATCC, catalog no. CCL-228) were cultivated in RPMI 1640 supplemented with 10% FBS, 2 mM glutamine and 0.05% gensumycin.

The human multiple myeloma cell lines INA-6, ANBL-6, and JJN3 were kind gifts from Dr M. Gramatzki (University of Erlangen-Nurnberg, Erlangen, Germany), Dr D. Jelinek (Mayo Clinic, Rochester, MN, USA), and Dr. J. Ball (University of Birmingham, UK), respectively, whereas RPMI-8226 and U266 were from ATCC (Rockville, MD, USA), and KJON was established in our laboratory {Vatsveen, 2016 #83;Burger, 2001 #84;Jelinek, 1993 #85;Jackson, 1989 #86}. INA-6, ANBL-6, and JJN3 were grown in RPMI supplemented with 10% FBS and 2 mM L-glutamine. RPMI-8226 and U266 were grown in RPMI supplemented with 2 mM glutamine, and 20% or 15% FBS, respectively. KJON cells were grown in RPMI supplemented with 10% human serum (HS) (Department of Immunology and Transfusion Medicine, St. Olav's University Hospital, Trondheim, Norway) and 2 mM L-glutamine. One ng/mL recombinant human interleukin (IL)-6 (Gibco, Thermo Fisher Scientific, Waltham, MA, USA), was added to the media of the IL-6 dependent myeloma cell lines INA-6, ANBL-6 and KJON. The cell lines were maintained at 37°C with 5% CO_2.

Bone marrow aspirates (n=6) were obtained from patients with AML (n=6) after informed consent, using protocols approved by a local institutional review board of Helsinki University Hospital and Comprehensive Cancer Center and in accordance with the Declaration of Helsinki. Mononuclear cells (MNCs) were isolated by density gradient separation (Ficoll-Paque PREMIUM; GE Healthcare, Little Chalfont, Buckinghamshire, UK) and immediately analyzed or vitally frozen for later use. Cells were maintained in mononuclear cell medium (MCM; Promocell, Heidelberg, Germany) or in a 25% HS-5 CM plus 75% RPMI 1640 medium mix. Cell viability was measured using the CellTiter-Glo (CTG) reagent (Promega, Madison, WI), according to the manufacturer's instructions, with a PHERAstar FS plate reader (BMG LABTECH, Ortenberg, Germany).

C. elegans maintenance, lifespan and toxicity assays

Standard *C. elegans* strain maintenance procedures were followed in all experiments (Brenner, 1974; Fang et al., 2019; Fang et al., 2016; Fang et al., 2014). Nematode rearing temperature was kept at 20 °C, unless noted otherwise. N2: wild type Bristol isolate was from Caenorhabditis Genetics Center (CGC).

For lifespan experiments, gravid adult worms were placed on NGM plates containing either A-1155463 (10 µM), 4NQO (10 µM), combination A-1155463 (10 µM) + 4NQO (10 µM) or vehicle control and seeded with OP50 to lay eggs. Progeny were grown at 20°C through the L4 larval stage and then transferred to fresh plates in groups of 30-35 worms per plate for a total of 100 individuals per experimental condition. Animals were transferred to fresh plates every 2–4 days thereafter and examined every other day for touch-provoked movement and pharyngeal pumping, until death.

Worms that died owing to internally hatched eggs, an extruded gonad or desiccation due to crawling on the edge of the plates were censored and incorporated as such into the data set. Survival curves were created using the product-limit method of Kaplan and Meier. The log-rank (Mantel–Cox) test was used for statistical analysis.

A series of toxicity experiments, including fecundity, egg hatching, larval development, were conducted using N2 Bristol isolate *C. elegans*, which were cultivated as previously described (Brenner, 1974) and maintained at 20°C. Briefly, for the toxicity assay animals were initially synchronised by bleaching gravid adults (adult day 1-4) to extract the eggs. Eggs were placed on nematode growth medium (NGM) plates seeded with *Escherichia coli* (OP50). L4 larvae were subsequently transferred onto fresh OP50-seeded NGM plates and allowed to grow to adulthood. Ten adult day 1 worms (n = 30-50/experimental condition) were transferred onto assay NGM plates with OP50 containing either A-1155463 (1, 10, 100 µM), 4NQO (1, 10, 100 µM), combination A-1155463 (10 µM) plus 4NQO (2, 10, 20 µM) or vehicle control. Animals laid eggs for three hours. Subsequently, adults were removed from the plate and the frequency of eggs laid was quantified as a measure of reproduction and egg-laying capacity of worms. The following day the frequency of unhatched eggs and L1 larvae were counted in order to evaluate the efficiency of egg hatching. Subsequently, 36 h later, development to L4 larvae was assessed, as a measure of larval growth. Finally, growth of L4 larvae to adulthood was quantified after 16 h.

The toxicity assay was conducted at 20°C on 10 ml NGM plates seeded with 100 µl OP50 from an overnight culture. Drug compounds and vehicle solvents were dissolved in a total volume of 200 µl, sufficient to cover the entire surface of the plate, and were dried at room temperature for 1-2 h prior to the transfer of worms. Each chemical concentration was tested three-five times. Statistical analysis was conducted using One-Way ANOVA followed by Tukey's multiple comparison test.

Real-time impedance assay

RPE cells were grown at 37°C in 16-well E-Plates to 90% confluency. The plates were supplied with golden electrodes at the bottom of the wells and a weak electrical current was constantly applied to the cell medium. The changes in the cell adherence indexes (CI) were monitored by the xCELLigence real-time drug cytotoxicity system (ACEA Biosciences, San Diego, USA) as described previously (Solly et al., 2004). When cells reached 90% confluency, 1 µM 4NQO, 1 µM A-1155463 or their combination were added. Control cells were treated with 0.01% of DMSO. CI were normalized and monitored for another 24 hours.

Cell viability assay

Approximately, $4x10^4$ RPE or HCT116 cells per well of 96-well plate were treated with A-1155463, 4NQO or both compounds. Control cells were treated with 0.01% of DMSO. After 24 or 48 h, respectively, the viability of cells was measured using the Cell Titer Glo assay (CTG, Promega). Luminescence was measured using PerkinElmer Victor X3 or Synergy Mx plate readers.

Cell toxicity assay

Approximately, $4x10^4$ HCT116, JJN3, ANBL6, U266, RPMI8226, KJON, and INA6 cells per well of 96-well plate were treated with 1 µM 4NQO, 1 µM A-1155463 or their combination. Control cells were treated with 0.01% of DMSO. After 24 h, the death of cells was detected using the Cell Toxicity Assay (CTxG, Promega). Fluorescence was measured using PerkinElmer Victor X3 Reader.

Early apoptosis assay

Approximately, $4x10^4$ RPE, HCT116 *TP53*$^{+/+}$ or HCT116 *TP53*$^{-/-}$ cells were seeded per well of 96-well plate and were treated with 1 µM 4NQO, 1 µM A-1155463 or their combination. Control cells were treated with 0.01% of DMSO. Activation of apoptosis was assessed using RealTime-Glo Annexin V Apoptosis and Necrosis Assay (Promega). Luminescence was measured using PerkinElmer Victor X3 Reader.

Apoptosis and phospho-kinase arrays

Approximately, $1x10^6$ RPE cells per well of 6-well plate were treated with 1 µM 4NQO, 1 µM A-1155463 or their combination. Control cells were treated with 0.01% of DMSO. After 2 h, relative levels of apoptosis-related proteins and protein kinase phosphorylation were determined using proteome profiler human apoptosis and human phospho-kinase array kits, respectively, as described in the manuals (R&D Systems, Minneapolis, MN, USA). Membranes were scanned using Odyssey Li-Cor system.

Metabolic labelling of cellular RNA and proteins

To label newly synthesised RNA or proteins, approximatel, $1x10^5$ RPE cells per well of 12-well plate were seeded and treated with 1 µM 4NQO, 1 µM A-1155463 or their combination dissolved in 500 µl cell growth medium. Control cells were treated with 0.01% of DMSO. The medium was supplemented with 3 µl of [alpha-P32]UTP (9,25 MBq, 250 µCi in 25 µl). Cells were incubated for 2 h at 37 °C. Cells were washed twice with PBS. Total RNA was isolated using RNeasy Plus extraction kit (Qiagen, Hilden, Germany). RNA was separated on 1% agarose gel. Gel was dried. Total RNA was detected using ethidium bromide. ^{32}P-labeled RNA was monitored using autoradiography and visualised using Typhoon 9400 scanner (GE Healthcare).

In a parallel experiment, the compounds or DMSO were added to 500 µl cysteine- and methionine-free DMEM medium (Sigma-Aldrich, Germany) containing 10% BSA and 3 µl [^{35}S] EasyTag Express protein labelling mix (7 mCi, 259 MBq, 1175 Ci/mmol in 632 ml; Perkin Elmer, Espoo, Finland). After 2 h of incubation at 37 °C cells were washed twice with PBS, lysed in 2 × SDS-loading buffer and sonicated. Lysates were loaded and proteins were separated on a 10% SDS-polyacrylamide gel. ^{35}S-labelled proteins were monitored using autoradiography and visualised using a Typhoon 9400 scanner (GE Healthcare).

UV radiation assay

RPE cells were exposed to UVC (λ = 254 nm) or to UVB (λ = 302 nm) using Hoefer UVC 500 Ultraviolet Crosslinker (20 J/cm^2) or VM25/30/GX trans-illuminator as UV sources, respectively. 1 µM A-1155463 or 0.1% DMSO were added to the cell medium. After 24 h viability of cells was measured using CTG assay (Promega, Madison, USA). The luminescence was read with a PHERAstar FS plate reader (BMG Labtech, Ortenberg, Germany).

Synergy calculations

Cells were treated with increasing concentrations of a Bcl-2 inhibitor and other drug, as indicated. After 24 h cell viability was measured using CTG assay. To test whether the drug combinations act synergistically, the observed responses were compared with expected combination responses. The expected responses were calculated based on Bliss reference model using SynergyFinder web-application (Ianevski et al., 2017). For in vitro combinatorial experiments where the whole dose-response matrix was measured, a normalized Bliss reference model, i.e. Zero Interaction Potency (ZIP) model was utilized. Unpaired t-test p-value was calculated using stats R package (v.3.6.3), to test the null hypothesis that no difference exists between synergy score mean values of two groups. We considered drug combinations with the synergy scores >7.5 as highly synergistic, and drug combinations with the synergy scores between 5 and 7,5 as moderately synergistic.

Fractionation of RPE cells

RPE cells were remained untreated or treated with 1 µM A-1155463, 1 µM 4NQO or their combination for 2 h. The cells were washed with PBS and collected in the cell lysis buffer consisting of 10 mM HEPES, pH 7.5, 10 mM KCl, 0.1 mM EDTA, 1 mM dithiothreitol, 0.5% Nonidet‑40 and protease inhibitor cocktail. The cells were placed on ice for 20 min with vortexed mix every 5 min, and then centrifuged at 12,000 g at 4°C for 10 min. The supernatant was collected as cytoplasmic fraction. Remaining cell pellets were washed three times with the cell lysis buffer and resuspended in the nuclear buffer consisting of 20 mM HEPES, pH 7.5, 400 mM NaCl, 1 mM EDTA, 1 mM dithiothreitol, protease inhibitor cocktail. The resuspended nuclear fraction was placed in ice for 30 min and centrifuged at 12,000 g at 4°C for 15 min. The supernatant was collected as nuclear extracts. Protein concentration of all cell fractions was determined using Bradford's reagent (BioRad, USA).

Analysis of mitochondrial membrane potential

RPE cells were remained untreated or treated with 1 µM A-1155463, 1 µM 4NQO or their combination for 2 h. The mitochondrial potential was determined using JC-1 dye staining according to the manufacturer's instruction (ThermoFisher Scientific). The cells were washed once with PBS and stained with 10 ug/ml of JC-1 dye in culture medium for 10 min. The images of JC-1 staining were

captured using EVOS fluorescence microscope and the mitochondrial potential was indicated by the shift of the fluorescence intensity ratio of J-aggregate (535/590 nm) and monomers (485/530 nm).

Immuno-precipitation and immuno-blotting

RPE cells were remained untreated or treated with 1 μM A-1155463, 1 μM 4NQO or their combination for 2 h. Cells were lysed in buffer containing 20 mM Tris-HCl, 0.5% NP-40, 150 mM NaCl, 1.5 mM $MgCl_2$, 10 mM KCl, 10% Glycerol, 0.5 mM EDTA, pH 7.9 and protease inhibitor cocktail (Sigma). Bcl-xL-associated factors were immuno-precipitated using rabbit anti-Bcl-xL antibody (54H6, Cell Signalling Technology) immobilized on the magnetic Protein G Dynabeads (Thermo Fisher Scientific). Normal rabbit IgG (Santa Cruz Biotechnology, sc-2025) was used to control immunoprecipitation with an equal volume of cell lysate. The immobilized protein complexes together with the appropriate whole-cell extract inputs were subjected for SDS-PAGE followed by immunoblotting.

Proteins were transferred to nitrocellulose membrane (Sartorius). The membranes were blocked with 10% BSA (Santa Cruz Biotechnology) in TBS. Primary antibodies (rabbit anti-Bax, SC-493, 1:1000; rabbit anti-BAD, sc-493, 1 : 1000; rabbit anti-Bad, D24A9, 1:1000; mouse anti-p53, sc-126, 1 : 1000; mouse anti-GAPDH, sc-32233; 1 : 1000 (Santa Cruz Biotechnology); goat anti-p53, af1355, 1:1000 (RnD Systems) anti-Bcl-xL, 1 : 1000, 54H6) were diluted in TBS and added to the membranes. After overnight incubation at 4 °C, membranes were washed three times with TBS buffer containing 0.03% Tween 20 (Tween/TBS). Secondary antibodies conjugated to HRP (Santa Cruz Biotechnology, anti-mouse: m-IgGκ BP-HRP, sc-516102; anti-rabbit mouse anti-rabbit IgG-HRP, sc-2357) were added. Chemiluminescence was detected using the Western Lightning Chemiluminescence Reagent (Perkin Elmer) by ChemiDoc Imaging System (BioRad).

HCT116 *TP53*$^{+/+}$ and *TP53*$^{-/-}$ cells remained untreated or were treated with 1 μM A-1155463, 1 μM 4NQO or both compounds. After 16 h, cells were lysed, and proteins were separated using 4-20% gradient SDS-PAGE. The proteins were transferred to a Hybond-LFP PVDF membrane. The membranes were blocked using 5% milk in Tris-buffered saline (TBS). p53 and GAPDH were detected using mouse anti-p53 and mouse anti-GAPDH antibodies as described above.

Confocal microscopy

RPE cells were treated with 1 μM A-1155463, 1 μM 4NQO or both compounds. Control cells were treated with 0,1% DMSO. After 1 and 2 h cells were fixed using 3.3% formaldehyde in 10% FBS and PBS, pH 7.4. Cells were permeabilized using 10% FBS and 0.1% Triton X-100 in PBS. Bad, Bax (2 different antibodies), Bcl-xL, p53 and Tom40 were detected using rabbit anti-Bcl-xL (1 : 250; clone 54H6; Cell Signalling Technology), mouse anti-Bax (1:250; 2D2, sc-20067), rabbit anti-Bax (1:250; N-20, sc-493), rabbit anti-BAD (1:250; clone D24A9; Santa Cruz Biotechnology), mouse anti-p53 (1 : 250; Santa Cruz Biotechnology) and anti-Tom40 (1:250; Santa Cruz Biotechnology, sc-11414) antibodies were used. Secondary goat anti-mouse IgG (H+L) Alexa Fluor® 488 and 568 (Thermo Scientific), goat anti-rabbit IgG (H+L) Alexa Fluor® 488 and 568 (Thermo Scientific) antibodies were

used. ProLong™ Gold Antifade Mountant (Invitrogen) with DAPI was used for mounting of cells. Cells were imaged using Zeiss LSM710 confocal microscope.

RESULTS

Toxicity of A-1155463-4NQO combination in *C. elegans*

We demonstrated recently that A-1155463 prematurely killed virus-infected or RNA/DNA-transfected cells via Bcl-xL-mediated apoptosis (Bulanova et al., 2017; Kakkola et al., 2013; Shim et al., 2017). We hypothesised that not only invasive RNA or DNA (biological factors) but also DNA/RNA-damaging chemical or physical factors could trigger apoptosis in A-1155463-sencitized cells. We tested DNA-damaging agent 4NQO (Walker and Sridhar, 1975) plus Bcl-xL-specific inhibitor A-1155463 in *C. elegans*. The worms treated with A-1155463-4NQO combination died faster than those treated with either A-1155463 or 4NQO (Fig. 2a, b). Moreover, the worms treated with the drug combination exhibited defects in reproduction and development (Fig. 2c). The Bliss synergy scores for adult development, L4 development and egg hatching were 19, 21 and 24, respectively. This synergy score can be interpreted as the average excess response due to drug interactions (i.e.,19, 21, and 24 % of cell survival beyond expected additivity between single drugs). Treatment with A-1155463 or 4NQO alone did not affect these stages. Thus, combination of 4NQO with A-1155463 had a severe impact on the *C. elegans* lifespan, reproductive system and development.

Toxicity of A-1155463-4NQO combination for human, monkey and dog cells

To recapitulate the *in vivo* toxicity of A-1155463-4NQO combination in *in vitro* experiments, we used human non-malignant retinal pigment epithelium (RPE) cells. The cells died 3 h after treatment with A-1155463-4NQO combination, whereas majority of cells treated with either A-1155463 or 4NQO remained viable for 24 h as measured by real-time impedance assay (Fig. 3a). Another cell viability assay, which quantified intracellular ATP, demonstrated that the effect of A-1155463-4NQO combination was synergistic (ZIP synergy score, 14±3; Fig. 3b). Similar results were obtained with 4NQO in combination with another Bcl-xL-specific inhibitor, A-133852 (ZIP synergy score, 17±0; Fig. 3c). ABT-263, a pan-Bcl-2 inhibitor, also showed synergy with 4NQO (ZIP synergy score, 8±1; Fig. 3c). In contrast, combinations of 4NQO with the Bcl-2- or Mcl-1-specific inhibitors did not show a synergy (ZIP synergy scores, 3±1 and 2±1, respectively; Fig. 2c). These results suggested that the DNA-damaging agent combined with Bcl-xL-, but not Bcl-2- or Mcl1-specific inhibitors facilitated the death of human non-malignant cells.

We also tested 4NQO-A-1155463 and 4NQO-A-1331852 combinations in three human cancer A549, H460 and Caco-2 cell lines and (Fig. 3d). In addition, we tested 4NQO-A-1155463 combination in a panel of patient-derived primary cell cultures (Fig. 3e), monkey Vero-E6 and dog MDCK cells (Fig. 3f). The combinations showed synergy in all tested cells, indicating that the DNA-damaging agent combined with Bcl-xL-specific inhibitor facilitated the death of monkey, dog, human non-malignant and malignant cells.

4NQO triggered overexpression of p53, A-1155463-mediated release of Bad and Bax from Bcl-xL, whereas concerted action of both agents led to MOMP and apoptisis

Immunoblot analysis of whole-cell extracts, nuclear and cytoplasm fractions showed that p53, a key regulator of DNA-damage response and Bcl-xL-dependent apoptosis, was over-expressed and accumulated in the nucleus of RPE cells after 2 h in response to 4NQO treatment (both as single agent and in combination; Fig. 4a). Confocal microscopy confirmed this observation (Fig. 4b, c). Immuno-precipitation of Bcl-xL-interacting partners showed that A-1155463 displaced Bad and Bax from Bcl-xL in RPE cells after 2 h of treatment (Fig. 4c). This is in agreement with previous observations that upon treatment with a Bcl-xL inhibitor, BAX localized to the outer mitochondrial membrane and dimerized with BAK to form the pores and induce MOMP (Kakkola et al., 2013; Lai et al., 2007).

We monitored MOMP with the membrane-permeant JC-1 dye. JC-1 dye exhibits potential-dependent accumulation in apoptotic mitochondria, indicated by a fluorescence emission shift from green to red. The treatment of RPE cells with 4NQO-A-1155463 combination for 4 h decreased the red/green fluorescence intensity ratio, when compared to non-, 4NQO- or A-1155463-treated cells (Fig. 4d,e). This result indicated that concerted action of DNA-damaging agent and Bcl-xL inhibitor led to MOMP.

Of note, treatment of RPE cells for 2 h with 4NQO, A-1155463 or their combination did not substantially affect general translation as well as expression levels of several apoptotic proteins (Fig. S1b,c). By contrast, RNA synthesis was affected by the combination (Fig. S1a,d). These effects could represent the immediate early responses to apoptosis.

p53 is required for A-1155463-4NQO synergy

To test the significance of p53 overexpression for A-1155463-4NQO synergy, we used malignant HCT116 TP53$^{-/-}$ cells, which lacked p53 expression (Fig. 5a). A-1155463-4NQO combination had substantially lower effect on viability, death and early apoptosis of TP53$^{-/-}$ cells (Fig. 5b-d). By contrast, A-1155463-4NQO combination killed malignant HCT116 TP53$^{+/+}$ cells, at the same concentrations as for RPE cells. These results indicated that p53 was essential for A-1155463-4NQO synergy.

We also tested 4NQO-A-1155463 combination in a panel of cancer cell lines with different p53 status (Fig. 5e). The cell lines were A549, NCIH460 (lung), Caco-2, SW480, HT29, SW620 (large intestine), JJN3, ANBL6, U266, RPMI8226, KJON, and INA6 (haematopoietic and lymphoid tissue). The experiment revealed high synergism (synergy scores >7,5) for the drug combination in A549, NCIH460, Caco-2, SW480, SW620, RPMI8226, and INA6 cells. Moderate synergism (synergy scores between 5 and 7,5) was observed in ANBL6 and U266 cells which had S241Y and A161T mutations in p53. 4NQO-A-1155463 combination showed no or low synergism (synergy scores < 5) in JJN3, KJON and INA6 cell lines, which have deletions in *TP53* gene as well as in HT29 cells with R273H mutation in p53. Thus, we mutation in TP53 could affect the A-1155463-4NQO synergy.

Chemical agents triggering p53-dependent Bcl-xL-mediated apoptosis

We next tested combinations of A-1155463, A-133852, ABT-199, and S63845 with 39 DNA, RNA and protein damaging agents in RPE cells. The experiment revealed that A-133852 and A-1155463 in combination with these agents were highly synergistic, indicating that Bcl-xL was essential for induction of apoptosis in non-malignant cells under chemical insults (Fig. 6a, b). Importantly, combinations with synergy scores >7.5 induced expression of p53 after 2 h of treatment (Fig. 6c). Interestingly, combinations of S63845 with Bcl-xL, but not Bcl-2 inhibitors were highly synergistic (cytotoxic) indicating that S63845 could damage Mcl-1 or another potential cellular target (Fig. 6d).

Moreover, screening of A-1331852 with 527 approved and emerging investigational anticancer agents revealed 64 combinations with synergy scores >7.5 (Table S2). The hit anticancer agents targeted mainly cellular DNA replication (i.e. amsacrine, SN38, cisplatin, mitoxantrone, etoposide, dactinomycin), RNA transcription (i.e. dinaciclib, THZ2, alvocidib, fludarabine), protein signalling (i.e. AMG-232, UCN-01, pictilisib, triciribine) or cytoskeleton (i.e. idasanutiin, indibulin, vinorelbine), and, therefore, damaged DNA, RNA and proteins (Fig. 6e). Thus, these agents induced p53-dependent Bcl-xL-mediated apoptosis, i.e. Bcl-xL was essential for induction of apoptosis in non-malignant cells treated with RNA, DNA or protein-damaging agents.

We further exploited Bcl-xL-mediated apoptosis for identification of chemical agents that damage cellular DNA, RNA or proteins. We tested library consisting of 48 drugs commonly dispensed in Norway as well as random library consisting of 50 safe-in-man broad-spectrum antiviral agents. We also tested monomeric bisbenzimidazole-pyrrole MB2Py(Ac), dimeric benzimidazole-pyrroles DB2Py(4) and DB2Py(5), as well as dimeric bisbenzimidazoles DBA(3), DBA(5), and DBA(7) on A-1155463-sensitized and non-sensitized RPE cells (Fig. S2). These 6 molecules were developed to bind minor groove of DNA (Ivanov et al., 2013; Koval et al., 2018).

We found that combination with bortezomib had a Bliss synergy score >7.5 indicating that bortezomib impaired protein degradation, which could be associated with accumulation of damaged proteins, which triggered Bcl-xL-mediated apoptosis (Kim et al., 2014). Several compounds, including birth-control drug 17α-ethynylestradiol, immunosuppressant cyclosporin, antiviral agent brincidofovir, as well as DNA-binding probe MB2Py(Ac), in combination with A-1155463 had moderate synergy (synergy scores between 5 and 7.5), indicating that they could also trigger Bcl-xL-mediated apoptosis (Fig. 7a-c).

We also tested combinations of A-1155463 with S63845, MB2Py(Ac), camptothecin, bortezomib or 17α-ethynylestradiol in human cancer A549, and H460 as well as monkey Vero-E6 and dog MDCK cells (Fig. 7d). Combinations of A-1155463 with S63845, camptothecin or bortezomib were as highly synergistic as in RPE cells (except for A-1155463-bortezomib combination in H460 cells). Thus, drugs damaging cellular macromolecules triggered apoptosis in different cell lines and types.

Physical factors triggering Bcl-xL-mediated apoptosis

We next exposed A-1155463-sensitized and non-sensitized RPE cells to UVB and UVC radiation, which similarly to the 4NQO treatment, induced lesions in DNA (Walker and Sridhar, 1975). After 24 h the cell viability was measured using the CTG assay. We observed that already 8 sec of UVB or UVC

exposure killed A-1155463-sensitized but not non-sensitized RPE cells (Bliss synergy scores: 31.2 and 23.8, respectively; Fig. 8a,b). Similar effect was observed in UVC-exposed A-1155463-sensitized cancer A549, H460 and Caco-2 cell lines (Fig. 8c). This indicated that UV triggered Bcl-xL-mediated apoptosis in non-malignant and malignant human cells.

DISCUSSION AND CONCLUSIONS

We showed recently that pan-Bcl-2 inhibitor ABT-263 accelerated killing of influenza virus-infected mice. Moreover, non-malignant cells infected with viruses or transfected with viral RNA or plasmid DNA were sensitive to Bcl-xL-specific inhibitor A-1155463 (Bulanova et al., 2017; Kakkola et al., 2013; Shim et al., 2017). This indicates that invasive RNA or DNA, i.e. biological factors, could trigger apoptosis, and that Bcl-xL could serve as 'safety fuse' controlling the process (Fig. 9).

Here, we demonstrated that DNA-damaging agent 4NQO killed human, monkey and dog cells, as well as small roundworms (*C. elegans*), which were sensitized with A-1155463. The killing was dependent on the concentration of both agents. The synergistic effect of 4NQO-A-1155463 combination in non-malignant cells was p53-dependent and was associated with the release of Bad and Bax from Bcl-xL. Our results suggest that intracellular receptors sensed damaged DNA, transmitted this information via p53 to anti-apoptotic Bcl-xL, which released pro-apoptotic Bax and Bad to trigger MOMP, which led to cell death. Thus, when concentration of DNA damages reached critical levels, Bcl-xL triggered apoptosis (Fig. 9).

Combinations of 4NQO with the Bcl-2- or Mcl-1-specific inhibitors did not show a synergy, suggesting that Bcl-xL has functional specialization in cells. Moreover, our results indicate that the Bcl-xL-mediated apoptotic pathway is evolutionary conserved (from *C.elegans* to *H. sapiens*). In addition, we identified other chemical triggers of Bcl-xL-mediated apoptosis. We showed that anticancer agents targeting DNA replication (i.e. amsacrine, SN38, cisplatin, mitoxantrone, etoposide, dactinomycin), RNA transcription (i.e. dinaciclib, THZ2, alvocidib, fludarabine), protein signalling (i.e. AMG-232, UCN-01, pictilisib, triciribine), protein quality control (i.e. bortezomib), or cytoskeleton (i.e. idasanutib, indibulin, vinoirelbine) killed cells sensitized with Bcl-xL-specific inhibitor. We also identified physical triggers of Bcl-xL-mediated apoptosis. We observed that already 8 sec of UVB or UVC exposure killed A-1155463-sensitized but not non-sensitized non-malignant and malignant cells. This indicated that UV triggered Bcl-xL-mediated apoptosis in A-1155463-sensitized cells.

Our results suggest that systemic treatment with combinations including pan-Bcl-2 or Bcl-xL-specific inhibitors could be harmful for cancer patients (similarly to mice and round worms), because patients are constantly exposed to radiation, chemicals, and viral infections. Thus, we identified adverse effects of combinational therapies, which included pan-Bcl-2 or Bcl-xL-specific inhibitors.

Our study could help to explain why clinical trials with 31 drug combinations containing pan-Bcl-2 inhibitor have been terminated, withdrawn or suspended. These include trials with ABT-263 plus bendamustine and rituximab in patients with relapsed diffuse large B cell lymphoma or ABT-263 plus abiraterone acetate with or without hydroxychloroquine in patients with progressive metastatic castrate refractory prostate cancer (NCT02471391, NCT01423539).

Locally induced Bcl-xL-mediated apoptosis, however, could have a clinical potential. For example, skin cancers could be treated with local Bcl-xL-specific inhibitor plus UV radiation, oncolytic virus infection or anticancer medication. Recent studies support this idea by showing, for example, that combination of radiotherapy with pan-Bcl-2 inhibitors ABT-737 and ABT-263 killed breast and small cell lung cancer cells *in vitro* (Table S3) (Li et al., 2019; Wu et al., 2014). Moreover, ABT-737 sensitized chronic lymphocytic leukaemia cells to reovirus and vesicular stomatitis oncolysis (Samuel et al., 2013). In this respect, antibody-Bcl-xL inhibitor conjugates or Bcl-xL PROTACs can be used to achieve tissue selectivity and targeted delivery of the compounds (Khan, Zhang et al. 2019, Wang, He et al. 2019, He, Zhang et al. 2020).

In conclusion, we identified chemical, physical and biological factors that induced Bcl-xL-mediated apoptosis. This could provide novel opportunities for discovery of therapeutic and adverse effects of anticancer medications as well as to identify conditions to prevent aging, and treat non- and communicable diseases, given that cells with high concentration of damaged DNA, RNA or proteins or with invasive DNA and RNA molecules would be eliminated from an organism receiving a Bcl-xL-specific inhibitor.

DATA AVAILABILITY

Supplementary Data are available online.

ACKNOWLEDGEMENT

We thank Hege Ramstad, Jelena Kiprovskaja, Rouan Yao, Kristine Misund, Alun Parson, Nadra J. Nilsen and Laivi Karu for assistance. We also thank the DDCB core facility supported by the University of Helsinki and Biocenter Finland. This work was supported by the European Regional Development Fund the Mobilitas Pluss Project [MOBTT39 to D.E.K.], HELSE SøR-ØST, the Research Council of Norway and Rosa Sløyfe, Norwegian Breast Cancer Society [2017056, 262175, 2020001, 207819 to E.F.F.], and Russian Foundation for Basic Research [19-04-00206 to A.L.Z.]. Funding for open access charge: University of Tartu. This manuscript has been posted on bioRxiv: https://biorxiv.org/cgi/content/short/2020.01.13.904714v1.

REFERENCES

Adams, C.M., Clark-Garvey, S., Porcu, P., and Eischen, C.M. (2018). Targeting the Bcl-2 Family in B Cell Lymphoma. Front Oncol *8*, 636.

Brenner, S. (1974). The genetics of Caenorhabditis elegans. Genetics *77*, 71-94.

Bulanova, D., Ianevski, A., Bugai, A., Akimov, Y., Kuivanen, S., Paavilainen, H., Kakkola, L., Nandania, J., Turunen, L., Ohman, T.*, et al.* (2017). Antiviral Properties of Chemical Inhibitors of Cellular Anti-Apoptotic Bcl-2 Proteins. Viruses *9*.

Casara, P., Davidson, J., Claperon, A., Le Toumelin-Braizat, G., Vogler, M., Bruno, A., Chanrion, M., Lysiak-Auvity, G., Le Diguarher, T., Starck, J.B.*, et al.* (2018). S55746 is a novel orally active BCL-2 selective and potent inhibitor that impairs hematological tumor growth. Oncotarget *9*, 20075-20088.

Chen, J., Jin, S., Abraham, V., Huang, X., Liu, B., Mitten, M.J., Nimmer, P., Lin, X., Smith, M., Shen, Y.*, et al.* (2011). The Bcl-2/Bcl-X(L)/Bcl-w inhibitor, navitoclax, enhances the activity of chemotherapeutic agents in vitro and in vivo. Mol Cancer Ther *10*, 2340-2349.

Denisova, O.V., Kakkola, L., Feng, L., Stenman, J., Nagaraj, A., Lampe, J., Yadav, B., Aittokallio, T., Kaukinen, P., Ahola, T.*, et al.* (2012). Obatoclax, saliphenylhalamide, and gemcitabine inhibit influenza a virus infection. J Biol Chem *287*, 35324-35332.

Elmore, S. (2007). Apoptosis: a review of programmed cell death. Toxicol Pathol *35*, 495-516.

Fang, E.F., Hou, Y., Palikaras, K., Adriaanse, B.A., Kerr, J.S., Yang, B., Lautrup, S., Hasan-Olive, M.M., Caponio, D., Dan, X.*, et al.* (2019). Mitophagy inhibits amyloid-beta and tau pathology and reverses cognitive deficits in models of Alzheimer's disease. Nat Neurosci *22*, 401-412.

Fang, E.F., Kassahun, H., Croteau, D.L., Scheibye-Knudsen, M., Marosi, K., Lu, H., Shamanna, R.A., Kalyanasundaram, S., Bollineni, R.C., Wilson, M.A.*, et al.* (2016). NAD+ Replenishment Improves Lifespan and Healthspan in Ataxia Telangiectasia Models via Mitophagy and DNA Repair. Cell Metab *24*, 566-581.

Fang, E.F., Scheibye-Knudsen, M., Brace, L.E., Kassahun, H., SenGupta, T., Nilsen, H., Mitchell, J.R., Croteau, D.L., and Bohr, V.A. (2014). Defective mitophagy in XPA via PARP-1 hyperactivation and NAD(+)/SIRT1 reduction. Cell *157*, 882-896.

Fernandez, A.F., Sebti, S., Wei, Y., Zou, Z., Shi, M., McMillan, K.L., He, C., Ting, T., Liu, Y., Chiang, W.C.*, et al.* (2018). Disruption of the beclin 1-BCL2 autophagy regulatory complex promotes longevity in mice. Nature *558*, 136-140.

Haikala, H.M., Anttila, J.M., Marques, E., Raatikainen, T., Ilander, M., Hakanen, H., Ala-Hongisto, H., Savelius, M., Balboa, D., Von Eyss, B.*, et al.* (2019). Pharmacological reactivation of MYC-dependent apoptosis induces susceptibility to anti-PD-1 immunotherapy. Nat Commun *10*, 620.

Ianevski, A., He, L., Aittokallio, T., and Tang, J. (2017). SynergyFinder: a web application for analyzing drug combination dose-response matrix data. Bioinformatics *33*, 2413-2415.

Ianevski, A., Zusinaite, E., Kuivanen, S., Strand, M., Lysvand, H., Teppor, M., Kakkola, L., Paavilainen, H., Laajala, M., Kallio-Kokko, H.*, et al.* (2018). Novel activities of safe-in-human broad-spectrum antiviral agents. Antiviral Res *154*, 174-182.

Ivanov, A.A., Susova, O.Y., Salyanov, V.I., Kirsanov, K.I., and Zhuze, A.L. (2013). A new series of biologically active DNA minor groove binders based on bisbenzimidazole and benzimidazole-pyrrole motives. Journal of Biomolecular Structure and Dynamics *31*.

Jeong, J.H., Oh, J.M., Jeong, S.Y., Lee, S.W., Lee, J., and Ahn, B.C. (2019). Combination Treatment with the BRAF(V600E) Inhibitor Vemurafenib and the BH3 Mimetic Navitoclax for BRAF-Mutant Thyroid Carcinoma. Thyroid *29*, 540-548.

Kakkola, L., Denisova, O.V., Tynell, J., Viiliainen, J., Ysenbaert, T., Matos, R.C., Nagaraj, A., Ohman, T., Kuivanen, S., Paavilainen, H.*, et al.* (2013). Anticancer compound ABT-263 accelerates apoptosis in virus-infected cells and imbalances cytokine production and lowers survival rates of infected mice. Cell Death Dis *4*, e742.

Kale, J., Osterlund, E.J., and Andrews, D.W. (2018). BCL-2 family proteins: changing partners in the dance towards death. Cell Death Differ *25*, 65-80.

Kim, S., Chen, J., Cheng, T., Gindulyte, A., He, J., He, S., Li, Q., Shoemaker, B.A., Thiessen, P.A., Yu, B.*, et al.* (2019). PubChem 2019 update: improved access to chemical data. Nucleic Acids Res *47*, D1102-D1109.

Kim, S.Y., Song, X., Zhang, L., Bartlett, D.L., and Lee, Y.J. (2014). Role of Bcl-xL/Beclin-1 in interplay between apoptosis and autophagy in oxaliplatin and bortezomib-induced cell death. Biochem Pharmacol *88*, 178-188.

King, A.C., Peterson, T.J., Horvat, T.Z., Rodriguez, M., and Tang, L.A. (2017). Venetoclax: A First-in-Class Oral BCL-2 Inhibitor for the Management of Lymphoid Malignancies. Ann Pharmacother *51*, 410-416.

Korycka-Wolowiec, A., Wolowiec, D., Kubiak-Mlonka, A., and Robak, T. (2019). Venetoclax in the treatment of chronic lymphocytic leukemia. Expert Opin Drug Metab Toxicol *15*, 353-366.
Koval, V.S., Arutyunyan, A.F., Salyanov, V.L., Klimova, R.R., Kushch, A.A., Rybalkina, E.Y., Susova, O.Y., and Zhuze, A.L. (2018). DNA sequence-specific ligands. XVII. Synthesis, spectral properties, virological and biochemical studies of fluorescent dimeric bisbenzimidazoles DBA(n). Bioorg Med Chem *26*, 2302-2309.
Kuivanen, S., Bespalov, M.M., Nandania, J., Ianevski, A., Velagapudi, V., De Brabander, J.K., Kainov, D.E., and Vapalahti, O. (2017). Obatoclax, saliphenylhalamide and gemcitabine inhibit Zika virus infection in vitro and differentially affect cellular signaling, transcription and metabolism. Antiviral Res *139*, 117-128.
Lai, P.B., Chi, T.Y., and Chen, G.G. (2007). Different levels of p53 induced either apoptosis or cell cycle arrest in a doxycycline-regulated hepatocellular carcinoma cell line in vitro. Apoptosis *12*, 387-393.
Li, H., Wang, H., Deng, K., Han, W., Hong, B., and Lin, W. (2019). The ratio of Bcl-2/Bim as a predictor of cisplatin response provides a rational combination of ABT-263 with cisplatin or radiation in small cell lung cancer. Cancer Biomark *24*, 51-59.
Samuel, S., Beljanski, V., Van Grevenynghe, J., Richards, S., Ben Yebdri, F., He, Z., Nichols, C., Belgnaoui, S.M., Steel, C., Goulet, M.L.*, et al.* (2013). BCL-2 inhibitors sensitize therapy-resistant chronic lymphocytic leukemia cells to VSV oncolysis. Mol Ther *21*, 1413-1423.
Shamas-Din, A., Kale, J., Leber, B., and Andrews, D.W. (2013). Mechanisms of action of Bcl-2 family proteins. Cold Spring Harb Perspect Biol *5*, a008714.
Shen, Q., Li, J., Mai, J., Zhang, Z., Fisher, A., Wu, X., Li, Z., Ramirez, M.R., Chen, S., and Shen, H. (2018). Sensitizing non-small cell lung cancer to BCL-xL-targeted apoptosis. Cell Death Dis *9*, 986.
Shim, J.M., Kim, J., Tenson, T., Min, J.Y., and Kainov, D.E. (2017). Influenza Virus Infection, Interferon Response, Viral Counter-Response, and Apoptosis. Viruses *9*.
Solly, K., Wang, X., Xu, X., Strulovici, B., and Zheng, W. (2004). Application of real-time cell electronic sensing (RT-CES) technology to cell-based assays. Assay Drug Dev Technol *2*, 363-372.
Timucin, A.C., Basaga, H., and Kutuk, O. (2019). Selective targeting of antiapoptotic BCL-2 proteins in cancer. Med Res Rev *39*, 146-175.
Ursu, O., Holmes, J., Bologa, C.G., Yang, J.J., Mathias, S.L., Stathias, V., Nguyen, D.T., Schurer, S., and Oprea, T. (2019). DrugCentral 2018: an update. Nucleic Acids Res *47*, D963-D970.
Walker, I.G., and Sridhar, R. (1975). Alkali-labile lesions in DNA from cells treated with methylating agents, 4-nitroquinoline-N-oxide, or ultraviolet light. Basic Life Sci *5A*, 29-30.
Wishart, D.S., Feunang, Y.D., Guo, A.C., Lo, E.J., Marcu, A., Grant, J.R., Sajed, T., Johnson, D., Li, C., Sayeeda, Z.*, et al.* (2018). DrugBank 5.0: a major update to the DrugBank database for 2018. Nucleic Acids Res *46*, D1074-D1082.
Wong, R.S. (2011). Apoptosis in cancer: from pathogenesis to treatment. J Exp Clin Cancer Res *30*, 87.
Wu, H., Schiff, D.S., Lin, Y., Neboori, H.J., Goyal, S., Feng, Z., and Haffty, B.G. (2014). Ionizing radiation sensitizes breast cancer cells to Bcl-2 inhibitor, ABT-737, through regulating Mcl-1. Radiat Res *182*, 618-625.

FIGURE LEGENDS

Figure 1. Introduction into inhibitors of Bcl-2 protein family members and their combinations with other anticancer drugs. (a) Analysis of structural similarities between inhibitors of Bcl-2 proteins using C-SPADE. (b) Literature analysis of targets for inhibitors of Bcl-2 proteins. (c) Developmental status of drug combinations containing Bcl-2 inhibitors. For more information, please visit bcl2icombi.info.

Figure 2. A combination of Bcl-xL- specific inhibitor A-1155463 and DNA-damaging agent 4NQO exhibits synergistic toxicities on lifespan, reproduction and development to the wild type roundworm *C. elegans*. (a) Kaplan-Meier survival curves and estimates of survival data (b) of worms challenged with 10 µM A-1155463, 10 µM 4NQO, drug combination or vehicle. The log-rank Mantel-Cox test was used for statistical analysis. (c) Toxicity detection for the different stages of *C. elegans* reproduction and development after the treatment with 10 µM A-1155463, 10 µM 4NQO or their combination (Mean ± SD). Dotted lines above combination bars represent the expected effect given by Bliss reference model.

Figure 3. Combination of DNA-damaging agent 4NQO with Bcl-xL-, but not Bcl-2- or Mcl-1-specific inhibitors, exhibit synergistic toxicities on human non-malignant RPE, cancer A549, H460, Caco-2 and mononuclear cells (MNCs) isolated from AML patients as well as on monkey Vero-E6 and dog MDCK cells. (a) Real-time impedance traces for RPE cells exposed to 1 µM 4NQO, 1 µM A-1155463 or their combination. Control trace represents cells exposed to 0.1% DMSO (Mean ± SD; n = 8). (b) The interaction landscapes of A-1155463-4NQO combination. It represents the net combinational effects on viability of RPE cells, as measured with CTG assays. (c) Synergy scores of combinations of 4NQO and 5 Bcl-2 inhibitors on RPE cells (Mean ± SD; n = 3). Cells were treated with increasing concentrations of a Bcl-2 inhibitor and 4NQO. After 24 h cell viability was measured using the CTG assay. Synergy scores were quantified based on the ZIP model. (d) Synergy scores for combinations of 4NQO and 2 Bcl-xL inhibitors on human cancer A549, H460, Caco-2 cells. Cells were treated with increasing concentrations of a Bcl-xL inhibitor and 4NQO. After 24 h cell viability was measured using the CTG assay. Synergy scores were quantified based on the ZIP model. (e) Synergy scores for 4NQO- A-1155463 combination on MNCs. Cells were treated with increasing concentrations of a A-1155463, 4NQO or both agents. After 24 h cell viability was measured using the CTG assay. Synergy scores were quantified based on the ZIP model. (f) Synergy scores for 4NQO-A-1155463 combination for Vero-E6 and MDCK cells. Cells were treated with increasing concentrations of a A-1155463, 4NQO or both agents. After 24 h cell viability was measured using the CTG assay. Synergy scores were quantified based on the ZIP model.

Figure 4. 4NQO induces p53 expression, while A-1155463 triggers release of pro-apoptotic Bad and Bax from Bcl-xL to initiate MOMP in RPE cells. (a) RPE cells were treated with 1 µM 4NQO, 1 µM A-1155463 or their combination. Control cells were treated with 0.1% DMSO. Nuclear and cytoplasm fractions were prepared. P53, Bcl-xL, Bax, XLF, PAXX and GAPDH were analysed using Western blotting. (b) RPE cells were treated as for (a). Two hours after treatment cells were fixed. P53 and Bcl-

xL were stained with corresponding antibodies. Nuclei were stained with DAPI. Cells were imaged using a confocal microscopy and representative images (n=8) were selected. Scale bar, 20 µm. (c) Quantification of the red signal in the cells. (d) RPE cells were treated as for (a). Whole cell extracts (WCE) were obtained 2 h after treatment. Proteins were immuno-precipitated by anti-Bcl-xL antibody. P53, Bcl-xL, Bad, Bax, and GAPDH were analysed using Western blotting in WCE and immunoprecipitates. (e) RPE cells were treated as for (a). The mitochondrial potential was determined using JC-1 dye staining. The images of JC-1 staining were captured using fluorescence microscope and the mitochondrial potential was indicated by the shift of the fluorescence intensity ratio of J-aggregate (535/590 nm) and monomers (485/530 nm). Representative images (n=3) were selected. Scale bar, 100 µm. (f) Quantification of the ratios between the green and red signals (indicative of mitochondrial membrane depolarization).

Figure 5. p53 is required for A-1155463-4NQO synergy. (a) HCT116 TP53-/- and TP53+/+ cells were treated with 1 µM 4NQO, 1 µM A-1155463 or their combination. Control cells were treated with 0.1% DMSO. 2 h after treatment p53 and GAPDH were analysed using western blotting of whole-cell extracts. (b) Cells were treated as for (a). Cell viability was measured by the CTG assay. Mean ± SD, n = 3. (c) Cells were treated as for (a). Cell death was measured by the CTxG assay. Mean ± SD, n = 3. (d) Cells were treated as for (a). Apoptosis was measured by the Annexin V assay. Mean ± SD, n = 3. (e) Table showing p53 status (acording to https://web.expasy.org/cellosaurus/) and sencitivity scores of A-1155463-4NQO combination for several cancer cell lines. (f) Ribbon representation of the p53-DNA complex focusing on residues at position 132, 161, and 241, which are mutated in some cell lines from (e) (PDB code 1TUP). These residues are shown in magenta.

Figure 6. Identification of anticancer agents, which trigger Bcl-xL-mediated apoptosis. (a) Heatmap showing synergy scores for combinations of four Bcl-2 inhibitors and 39 anticancer agents. RPE cells were treated with 0, 10, 30, 100, 300, 1000, 3000 and 10000 nM Bcl-2 inhibitors and anticancer agents. After 24 h cell viability was measured by the CTG assay. (b) Distribution of synergy scores based on (a). (c) Immunoblot analysis of p53 and GAPDH (loading control) expression levels after 2h of treatment of RPE cells with selected anticancer agents. (d) Heatmap showing synergy scores for combinations of four Bcl-2 inhibitors with each other. RPE cells were treated with 0, 10, 30, 100, 300, 1000, 3000 and 10000 nM Bcl-2 inhibitors. After 24 h cell viability was measured by the CTG assay. (e) Cellular targets of anticancer agents which showed synergy with A-133852. RPE cells were treated with A-133852 and 527 anticancer agents as for panel (a). After 24 h cell viability was measured using the CTG assay. The compounds with synergy >7.5 were selected and plotted against their targets. ZIP method was used to calculate synergy scores for all panels.

Figure 7. Identification of chemical agents, which trigger Bcl-xL-mediated apoptosis. (a) Bliss synergy scores for A-1155463 and 48 commonly dispensed drugs. A-1155463-sensitized (1 µM) and non-sensitized (0.1% DMSO) RPE cells were treated with 0, 0.1, 0.4, 1.2, 3.7, 11.1, 33.3, and 100 µM of drugs. After 24 h cell viability was measured by the CTG assay (n=3). (b) Bliss synergy scores for A-

1155463 and 50 safe-in-man broad-spectrum antiviral agents. A-1155463-sensitized (1 μM) and non-sensitized (0.1% DMSO) RPE cells were treated with 0, 0.04, 0.12, 0.37, 1.11, 3.33, 10, and 30 μM of antiviral agents. After 24 h cell viability was measured by the CTG assay (n=3). (c) Bliss synergy scores for A-1155463 and DNA-binding agents. A-1155463-sensitized (1 μM) and non-sensitized (0.1% DMSO) RPE cells were treated with different concentrations of dimeric bisbenzimidazoles DBA(3), DBA(5) and DBA(7), monomeric bisbenzimidazole-pyrrole MB2Py(Ac) and dimeric benzimidazole-pyrroles DB2Py(4) and DB2Py(5). (d) Synergy scores of drug combinations for Vero-E6, MDCK, A549 and NCI-H460 cells. Cells were treated with increasing concentrations of a A-1155463, another agent or both agents. After 24 h cell viability was measured using the CTG assay. Synergy scores were quantified based on the ZIP model.

Figure 8. Identification of physical factors, which trigger Bcl-xL-mediated apoptosis. (a,b) RPE cells were exposed to UVB or UVC radiation for the indicated times and covered with medium containing 1 μM A-1155463 or 0.1% DMSO. After 24 h, viability of cells was measured using the CTG assay. Mean ± SD, n = 3. (c) Synergy scores of A-1155463-UVC combinations in 4 cell lines. Cells were treated with increasing A-1155463 concentrations and exposed UVC radiation for 0, 20, 40, 80, 160, and 240 sec. After 24 h cell viability was measured using the CTG assay. Synergy scores were quantified using Bliss model.

Figure 9. Schematic diagram showing how apoptosis could be initiated in response to chemical and physical stimuli or viruses, and how Bcl-xL-specific inhibitors could facilitate this process. Damage response (DR) factors and pattern recognition receptors (PRRs) recognize damaged molecules and invasive DNA or RNA, respectively. These proteins transduce signals to Bcl-xL via p53 or other protein(s). Pro-apoptotic Bax and Bad are released from anti-apoptotic Bcl-xL. When concentration of damaged or invasive molecules reach critical level, released Bax and Bad trigger mitochondrial outer membrane permeabilization (MoMP), which lead to inhibition of ATP synthesis, irreversible release of intermembrane space proteins, and subsequent caspase activation. This results in cell death. Alternatively, DR proteins and PRRs could mediate repair or degradation of damaged or invasive molecules, respectively, which would leave cells alive. Bcl-xL-specific inhibitors facilitate death of cells and, thus, impair repair or degradation of damaged or invasive factors.

FIGURES

Figure 1.

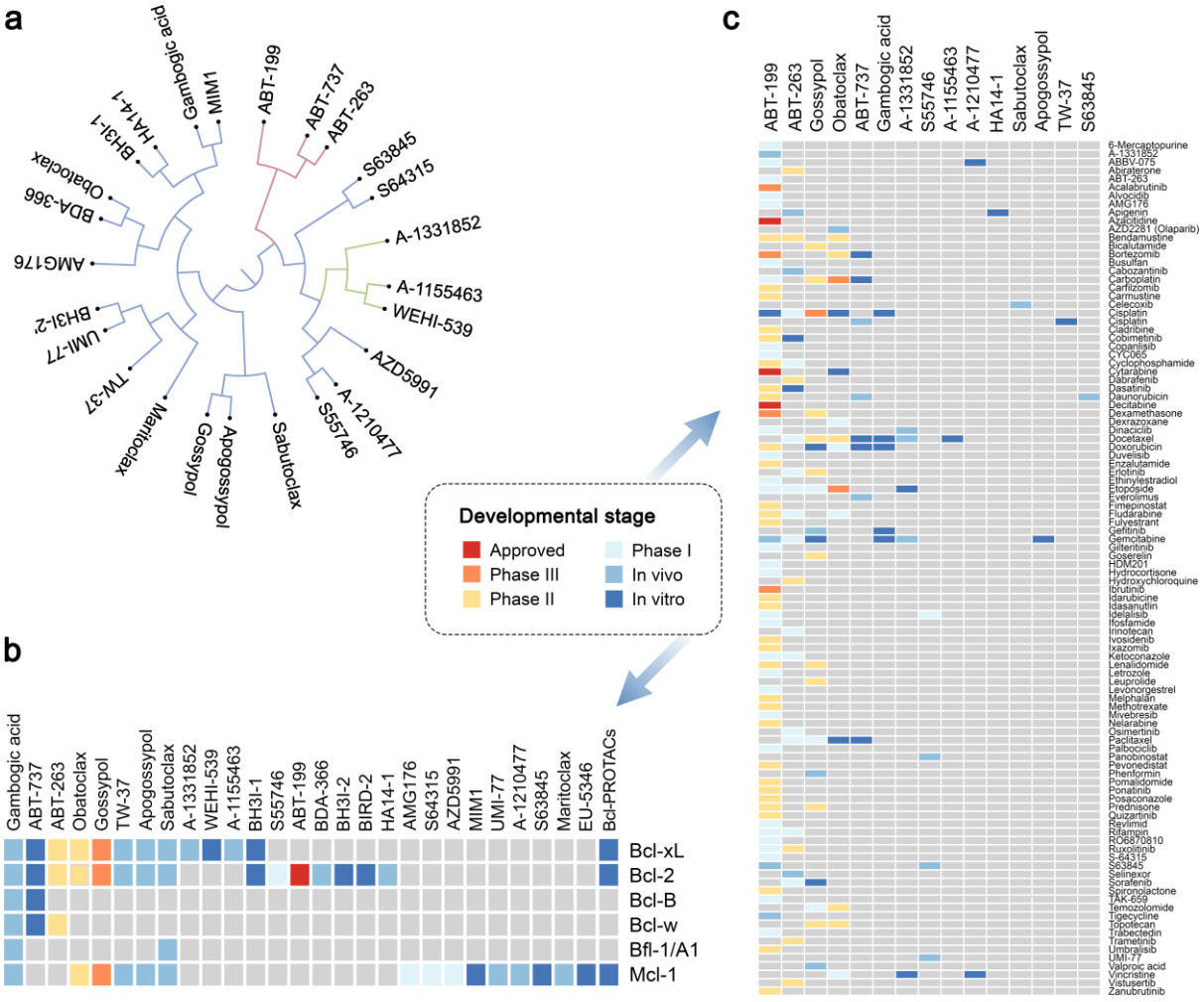

Figure 2.

a

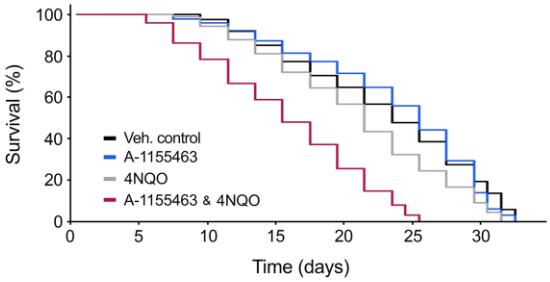

b

	Veh	A-1155463	4NQO	A-1155463+4NQO
Minimum	9	7	7	5
Median	23	25	21	15
Maximum	32	32	31	25
Mean	22.55	23.19	20.58	15.34
Std. Deviation	6.787	6.54	6.486	5.738
Std. Error of Mean	0.724	0.648	0.684	0.568

c

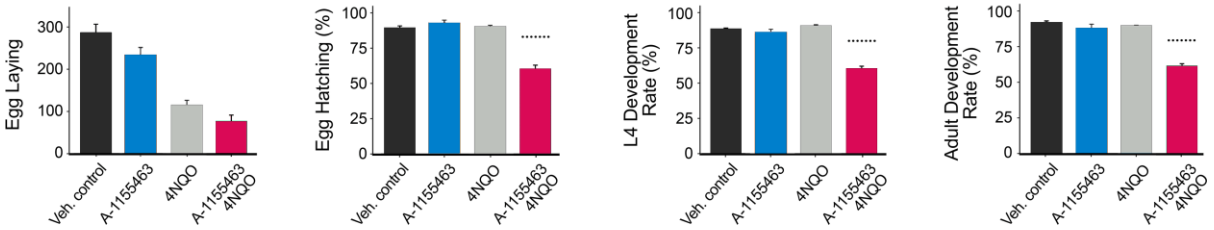

Figure 3.

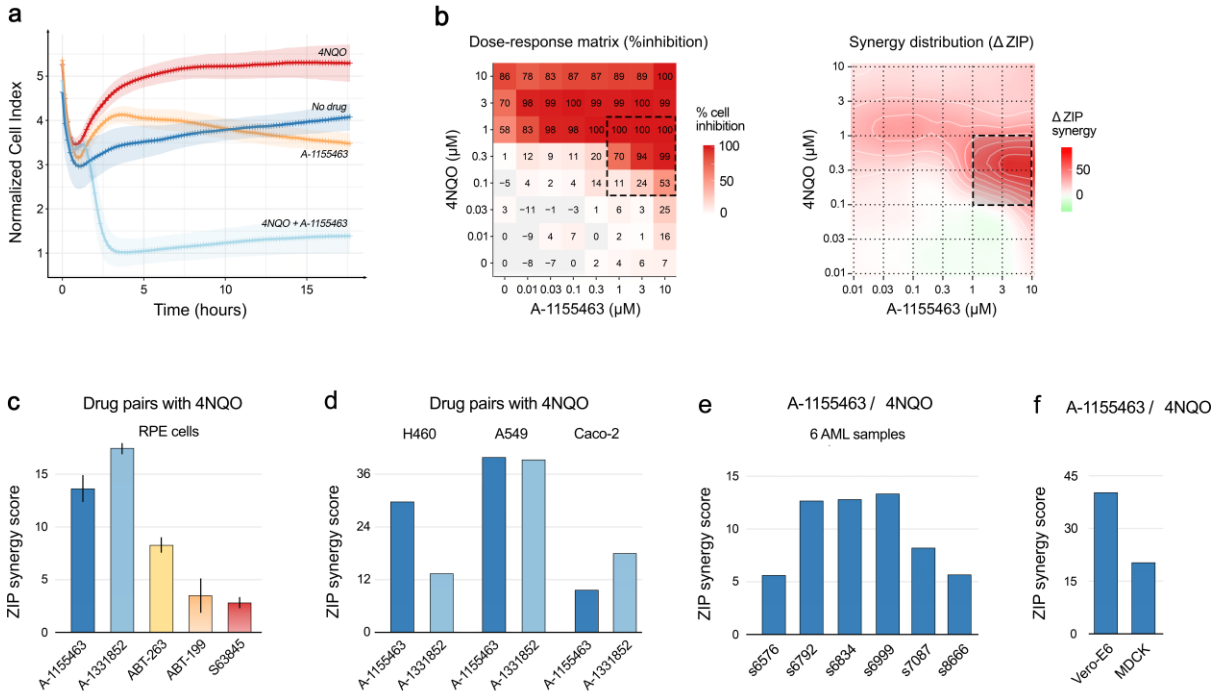
a
Normalized Cell Index
Time (hours)
4NQO
No drug
A-1155463
4NQO + A-1155463
b
Dose-response matrix (%inhibition)
4NQO (μM)
A-1155463 (μM)
% cell inhibition
Synergy distribution (Δ ZIP)
Δ ZIP synergy
c
Drug pairs with 4NQO
RPE cells
ZIP synergy score
A-1155463
A-1331852
ABT-263
ABT-199
S63845
d
Drug pairs with 4NQO
H460
A549
Caco-2
e
A-1155463 / 4NQO
6 AML samples
s6576
s6792
s6834
s6999
s7087
s8666
f
A-1155463 / 4NQO
Vero-E6
MDCK

Figure 4.

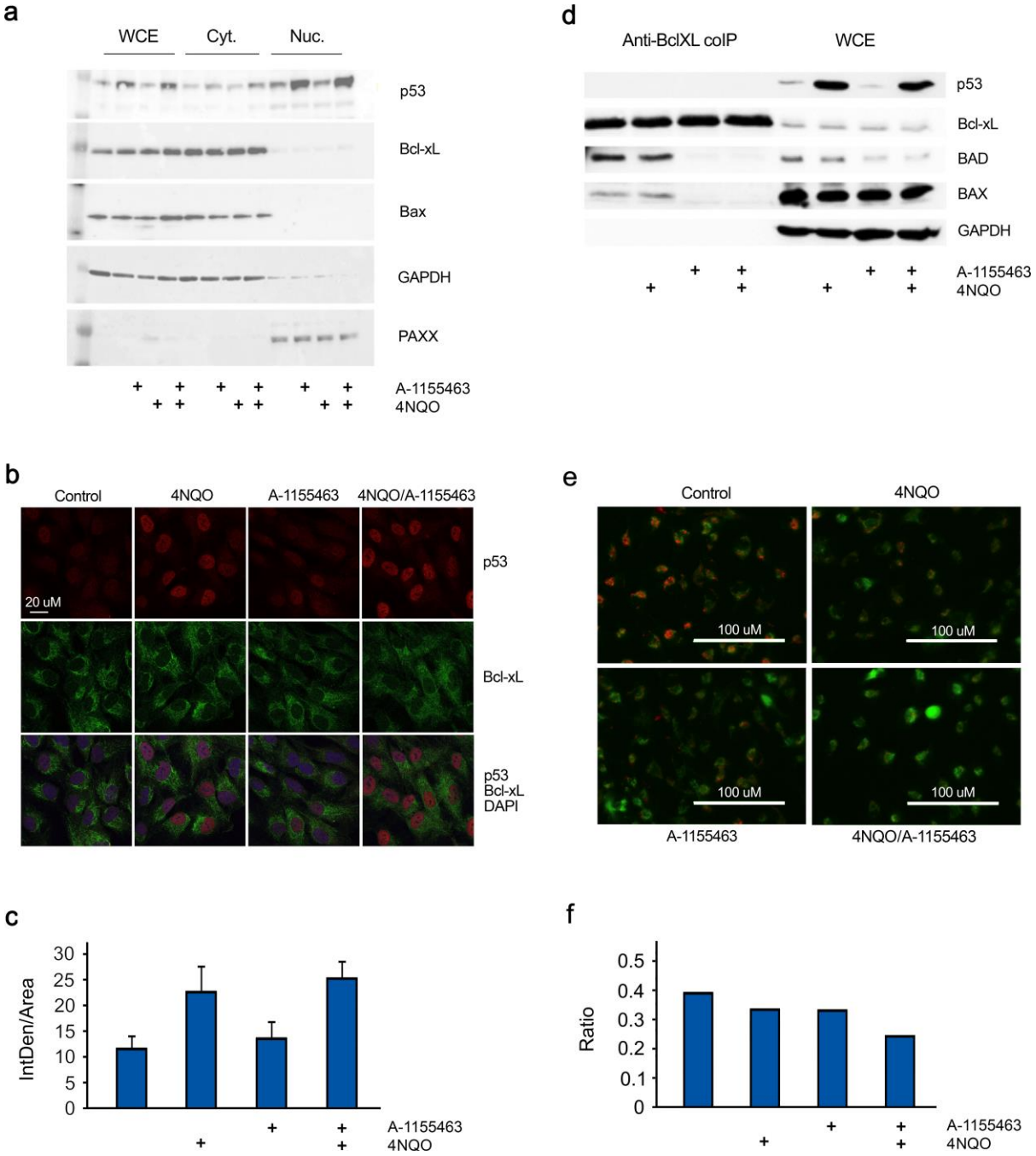
a
WCE
Cyt.
Nuc.
p53
Bcl-xL
Bax
GAPDH
PAXX
A-1155463
4NQO
d
Anti-BclXL coIP
WCE
p53
Bcl-xL
BAD
BAX
GAPDH
A-1155463
4NQO
b
Control
4NQO
A-1155463
4NQO/A-1155463
20 uM
p53
Bcl-xL
p53
Bcl-xL
DAPI
e
Control
4NQO
100 uM
A-1155463
4NQO/A-1155463
c
IntDen/Area
A-1155463
4NQO
f
Ratio
A-1155463
4NQO

Figure 5.

a

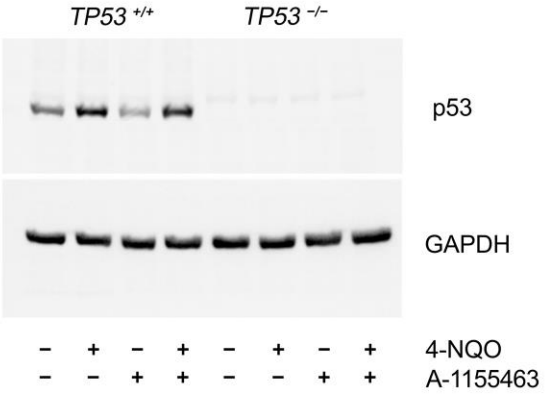

b

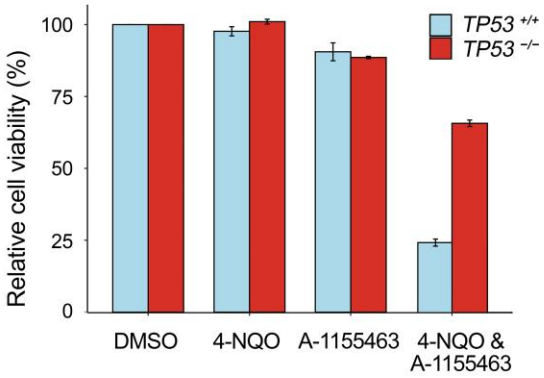

c

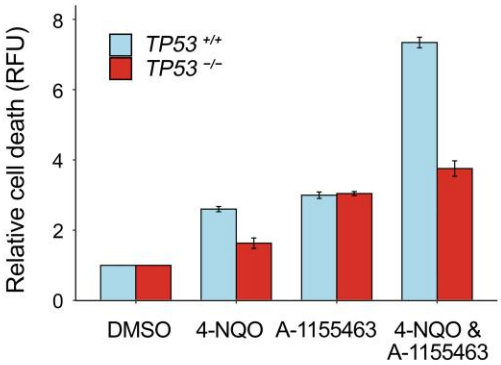

d

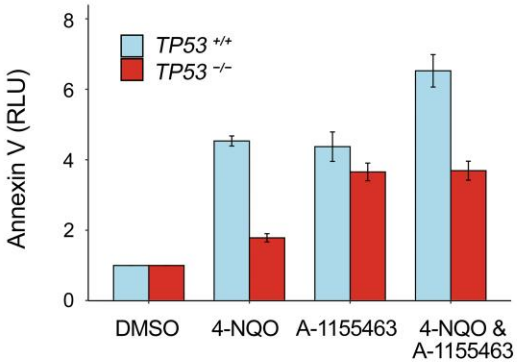

e

Cell line	TP53 mutations	Synergy score	MSA score
A549		39.43	57.99
NCIH46		29.833	54.12
CACO2	C135F	17.719	30.01
SW480	R273H, P309S	15.829	27.923
SW620	R273H, P309S	10.942	26.535
RPMI8226	E285K	10.237	14.27
ANBL6	S241Y	6.611	8.66
U266	A161T	6.555	8.14
HT29	R273H	3.196	10.931
INA6	K132M, Q331*	2.374	6.34
KJON	Y234*	2.305	5.17
JJN3	*del*	-0.013	2.33

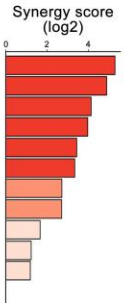

f

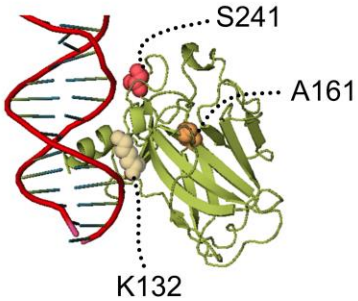

Figure 6.

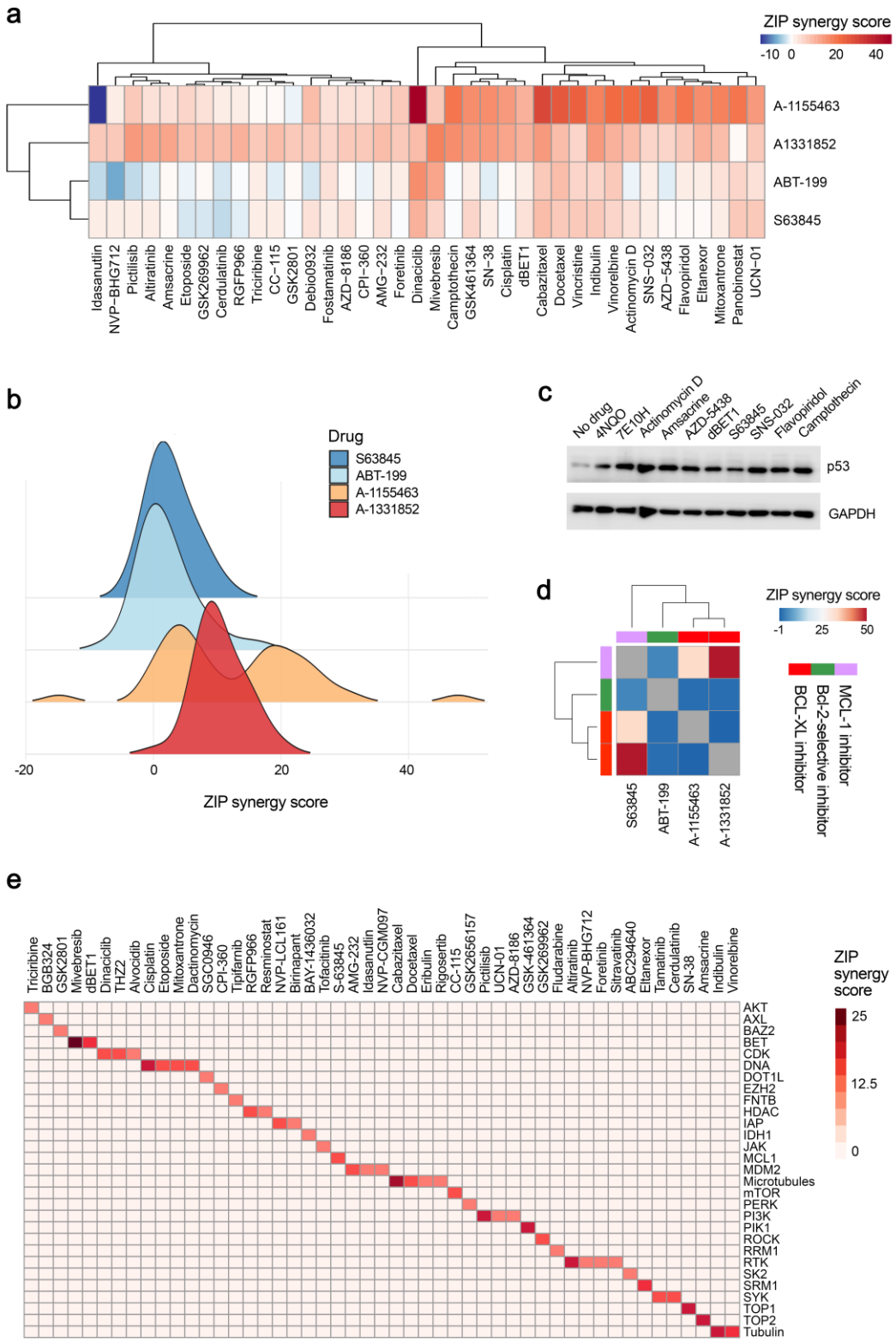
a
ZIP synergy score
-10 0 20 40
A-1155463
A1331852
ABT-199
S63845
Idasanutlin
NVP−BHG712
Pictilisib
Altiratinib
Amsacrine
Etoposide
GSK269962
Cerdulatinib
RGFP966
Triciribine
CC−115
GSK2801
Debio0932
Fostamatinib
AZD−8186
CPI−360
AMG−232
Foretinib
Dinaciclib
Mivebresib
Camptothecin
GSK461364
SN−38
Cisplatin
dBET1
Cabazitaxel
Docetaxel
Vincristine
Indibulin
Vinorelbine
Actinomycin D
SNS−032
AZD−5438
Flavopiridol
Eltanexor
Mitoxantrone
Panobinostat
UCN−01
b
Drug
S63845
ABT-199
A-1155463
A-1331852
-20
0
20
40
ZIP synergy score
c
No drug
4NQO
7E10H
Actinomycin D
Amsacrine
AZD-5438
dBET1
S63845
SNS-032
Flavopiridol
Camptothecin
p53
GAPDH
d
ZIP synergy score
-1 25 50
S63845
ABT-199
A-1155463
A-1331852
BCL-XL inhibitor
Bcl-2-selective inhibitor
MCL-1 inhibitor
e
Triciribine
BGB324
GSK2801
Mivebresib
dBET1
Dinaciclib
THZ2
Alvocidib
Cisplatin
Etoposide
Mitoxantrone
Dactinomycin
SGC0946
CPI-360
Tipifarnib
RGFP966
Resminostat
NVP-LCL161
Birinapant
BAY-1436032
Tofacitinib
S-63845
AMG-232
Idasanutlin
NVP-CGM097
Cabazitaxel
Docetaxel
Eribulin
Rigosertib
CC-115
GSK2656157
Pictilisib
UCN-01
AZD-8186
GSK-461364
GSK269962
Fludarabine
Altiratinib
NVP-BHG712
Foretinib
Sitravatinib
ABC294640
Eltanexor
Tamatinib
Cerdulatinib
SN-38
Amsacrine
Indibulin
Vinorelbine
AKT
AXL
BAZ2
BET
CDK
DNA
DOT1L
EZH2
FNTB
HDAC
IAP
IDH1
JAK
MCL1
MDM2
Microtubules
mTOR
PERK
PI3K
PIK1
ROCK
RRM1
RTK
SK2
SRM1
SYK
TOP1
TOP2
Tubulin
ZIP synergy score
25
12.5
0

Figure 7.

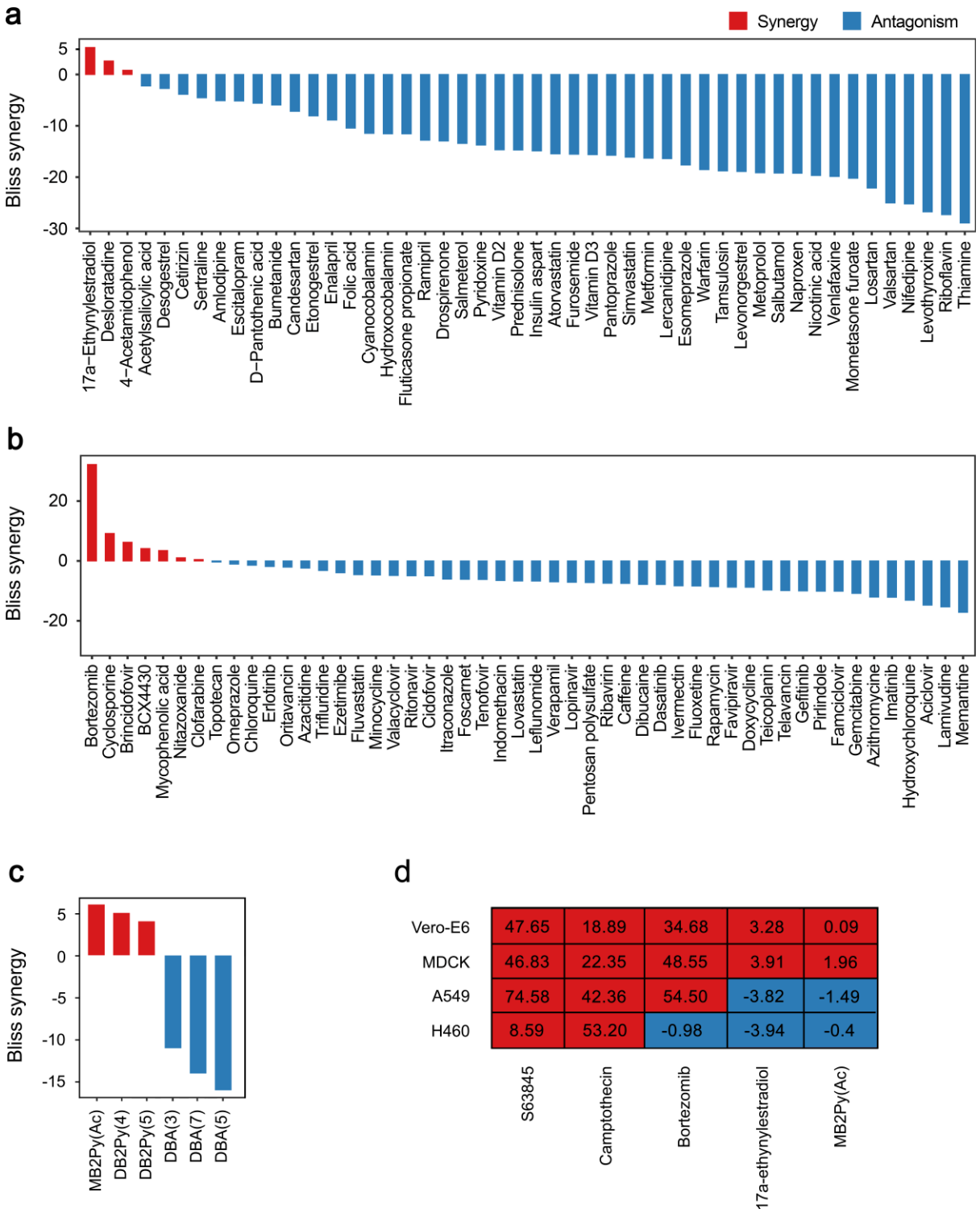
a
Synergy
Antagonism
Bliss synergy
5
0
-10
-20
-30
17a−Ethynylestradiol
Desloratadine
4−Acetamidophenol
Acetylsalicylic acid
Desogestrel
Cetirizin
Sertraline
Amlodipine
Escitalopram
D−Pantothenic acid
Bumetanide
Candesartan
Etonogestrel
Enalapril
Folic acid
Cyanocobalamin
Hydroxocobalamin
Fluticasone propionate
Ramipril
Drospirenone
Salmeterol
Pyridoxine
Vitamin D2
Prednisolone
Insulin aspart
Atorvastatin
Furosemide
Vitamin D3
Pantoprazole
Simvastatin
Metformin
Lercanidipine
Esomeprazole
Warfarin
Tamsulosin
Levonorgestrel
Metoprolol
Salbutamol
Naproxen
Nicotinic acid
Venlafaxine
Mometasone furoate
Losartan
Valsartan
Nifedipine
Levothyroxine
Riboflavin
Thiamine
b
Bliss synergy
20
0
-20
Bortezomib
Cyclosporine
Brincidofovir
BCX4430
Mycophenolic acid
Nitazoxanide
Clofarabine
Topotecan
Omeprazole
Chloroquine
Erlotinib
Oritavancin
Azacitidine
Trifluridine
Ezetimibe
Fluvastatin
Minocycline
Valacyclovir
Ritonavir
Cidofovir
Itraconazole
Foscarnet
Tenofovir
Indomethacin
Lovastatin
Leflunomide
Verapamil
Lopinavir
Pentosan polysulfate
Ribavirin
Caffeine
Dibucaine
Dasatinib
Ivermectin
Fluoxetine
Rapamycin
Favipiravir
Doxycycline
Teicoplanin
Telavancin
Gefitinib
Pirlindole
Famciclovir
Gemcitabine
Azithromycine
Imatinib
Hydroxychloroquine
Aciclovir
Lamivudine
Memantine
c
Bliss synergy
5
0
-5
-10
-15
MB2Py(Ac)
DB2Py(4)
DB2Py(5)
DBA(3)
DBA(7)
DBA(5)
d
Vero-E6 47.65 18.89 34.68 3.28 0.09
MDCK 46.83 22.35 48.55 3.91 1.96
A549 74.58 42.36 54.50 -3.82 -1.49
H460 8.59 53.20 -0.98 -3.94 -0.4
S63845
Camptothecin
Bortezomib
17a-ethynylestradiol
MB2Py(Ac)

Figure 8.

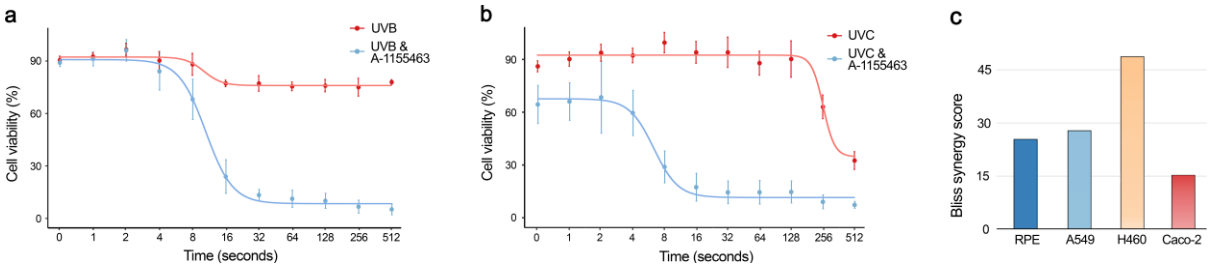
a
UVB
UVB &
A-1155463
Cell viability (%)
90
60
30
0
0
1
2
4
8
16
32
64
128
256
512
Time (seconds)
b
UVC
UVC &
A-1155463
Cell viability (%)
90
60
30
0
0
1
2
4
8
16
32
64
128
256
512
Time (seconds)
c
Bliss synergy score
45
30
15
0
RPE
A549
H460
Caco-2

Figure 9.

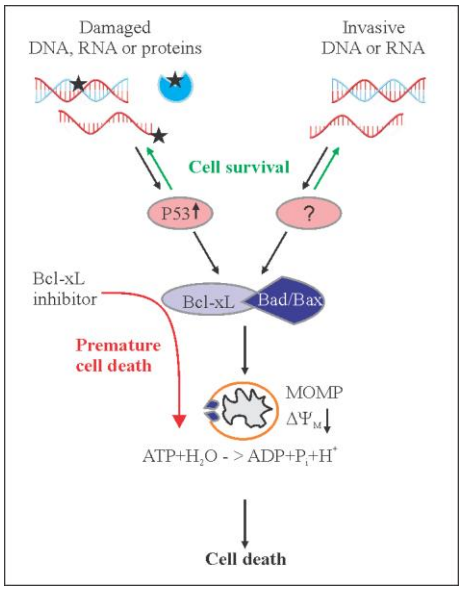
Damaged
DNA, RNA or proteins
Invasive
DNA or RNA
Cell survival
P53
?
Bcl-xL
inhibitor
Bcl-xL
Bad/Bax
Premature
cell death
MOMP
$\Delta\Psi_M$
$ATP+H_2O$ - > $ADP+P_i+H^+$
Cell death